

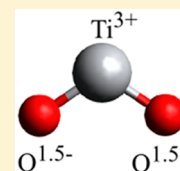
On the Charge State of Titanium in Titanium Dioxide

Daniel Koch and Sergei Manzhos*

Department of Mechanical Engineering, National University of Singapore, 9 Engineering Drive 1, Singapore 117576, Singapore

 Supporting Information

ABSTRACT: The oxidation state of titanium in titanium dioxide is commonly assumed to be +4. This assignment is based on the ionic approximation and is used ubiquitously to rationalize phenomena observed with TiO_2 . It implies a charge state +4 and that no further oxidation of the metal center is possible. We present a comprehensive electronic structure investigation of Ti ions, TiO_2 molecules, and TiO_2 bulk crystals using different density functional theory and wave function-based approaches, which shows that the charge state of Ti is +3. Specifically, there is evidence of a significant remaining contribution from valence s and d electrons of Ti, including the presence of a nuclear cusp around the Ti core. The charge corresponding to valence s and d states of Ti amounts to 1 e. This suggests the possibility of further oxidation of Ti in TiO_2 compounds and challenges the commonly assumed picture of assigning the oxidation state of Ti in titania to +4.



Titanium dioxide (TiO_2) is a material widely used in numerous technologies. TiO_2 polymorphs are large-band-gap semiconductors, which makes them suitable for applications in photocatalysis and solar cells^{1–3} and as promising electrode materials for Li-ion and Na-ion batteries due to their potentially high capacity, cycling stability, and charge/discharge rate.^{4,5} The band structure of titania compounds was reported extensively, commonly describing the valence band as being primarily composed of O 2p states and the conduction band mostly consisting of Ti 3d contributions.^{6,7} At the same time, the density of states shows other less important contributions, notably from Ti 3d states in the valence band.^{8,9}

The commonly accepted picture of the ionic oxidation states in TiO_2 is a quadruply charged Ti^{4+} cation held together with O^{2-} anions by highly ionic bonds, an assumption based on qualitative MO considerations.^{10,11} Indeed, the often-cited basis for the assumption of Ti^{4+} , photoelectron spectroscopy, relied on these very considerations to interpret XPS peaks.^{12,13} There does not seem to be direct, independent experimental evidence of the absolute charge or oxidation state. More recent quantum chemical computations, on the other hand, predict the mentioned 3d contributions to the TiO_2 valence band and an additional small fraction of 4s states in periodic titania systems. Furthermore, several charge analysis techniques such as Mulliken¹⁴ or Bader¹⁵ charge analysis predict a significant charge remainder at the Ti centers in TiO_2 polymorphs, suggesting Ti–O bonds with stronger covalent character.^{16,17} The computed charge states significantly lower than +4 are usually assumed to result from the (imperfect) definitions of charge transfer measures and have not led to questioning of the assumed Ti^{4+} state. The assumption of Ti^{4+} is used ubiquitously to rationalize phenomena observed with TiO_2 and related materials, such as doping or Li/Na insertion, which are said to lead to the formation of Ti^{3+} states.^{18,19} While the commonly used definition of the oxidation state does not require equal charge and oxidation state,²⁰ it implies a charge state of +4 and no possibility of further oxidation. The aim of this work is to analyze the electronic structure of titania, systematically

compare different charge measures on different titania systems, and, most importantly, quantify the remaining charge on the Ti centers in those systems independently of the shortcomings of common charge partitioning schemes. In some cases, assignment of computed charges can reliably be made to charge states significantly different from nominal charges returned by Mulliken or Bader charges; see, for example, refs 21 and 22. Should the nominal computed charges of Ti in TiO_2 , which are very different from +4, be still assigned to Ti^{4+} ? In this work, we establish a charge state of +3 in a way that may question the common assumption about the Ti oxidation state.

We proceeded as follows: First, spherically averaged densities of a single Ti atom in different oxidation states were compared among each other and with different methods for a comparison of the valence densities obtained from DFT and wave function-based methods and to determine characteristic features of the density distribution, such as evidence of the nuclear cusp. Second, spherically averaged densities for single TiO_2 molecules were analyzed and different charge analyses (Mulliken, Bader, Hirshfeld²³) applied, again with different methods, to quantify the charge remainder at the Ti center. Last, density distributions and charge remainders were computed for the periodic titania systems rutile and anatase to give an estimation of the atomic charge of Ti in solid TiO_2 compounds. Additionally, cumulative charges obtained as charge density integrated over the radial distance from the Ti centers were computed to verify the charge analysis schemes and to relate the spherically averaged density profile and the band structure to the Ti charge state in titania. We conclude that a valence charge corresponding to one electron remains on Ti within a radius significantly smaller than the Ti–O bond length; the charge state is therefore +3, raising the question about the appropriateness of the ionic model as a basis for conceptual understanding of the Ti oxidation state in TiO_2 .

Received: February 9, 2017

Accepted: March 21, 2017

Published: March 21, 2017

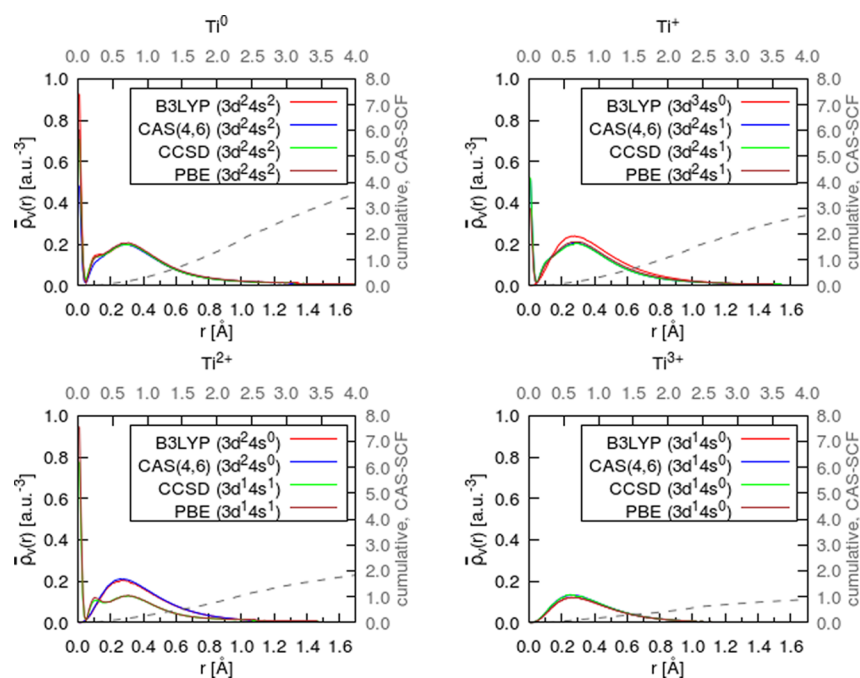


Figure 1. Spherically averaged valence electron density of neutral and cationic Ti species obtained with B3LYP, CAS(4,6), CCSD, and PBE with the cc-pVDZ basis set. The spatial coordinate r corresponds to the radial distance from the Ti center. The gray, dashed lines indicate the cumulative numbers of electrons within the spheres of corresponding radius (which converge at $r \rightarrow \infty$ to 4, 3, 2, and 1 e for Ti^0 , Ti^+ , Ti^{2+} , and Ti^{3+} , respectively).

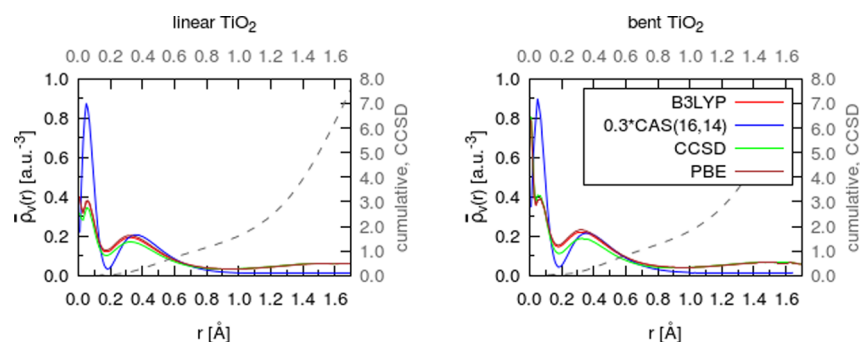


Figure 2. Spherically averaged valence electron density of a linear and bent TiO_2 molecule obtained with B3LYP, CAS(14,16), CCSD, and PBE with the cc-pVDZ basis set. The spatial coordinate r corresponds to the radial distance from the Ti center. The gray, dashed lines indicate the cumulative numbers of electrons within the spheres of corresponding radius. The CAS(16,14) curve is scaled by a factor of 0.3 for a better comparison.

Spherically averaged valence densities for a single Ti center in different oxidation states are shown in Figure 1 for B3LYP, CAS(4,6), CCSD, and PBE employing the cc-pVDZ basis set (see the Computational Details in the Supporting Information). Their lowest-energy valence configuration is indicated after the method name. The expected ground states for Ti , Ti^+ , Ti^{2+} , and Ti^{3+} are ^3F (valence configuration $3d^24s^2$), ^4F ($3d^24s^1$), ^3F ($3d^24s^0$), and ^2D ($3d^14s^0$).^{24,25} As can be seen from Figure 1, CAS-SCF is the only method that is capable of predicting the correct ground states of both Ti^+ and Ti^{2+} due to the multiconfigurational character of the wave functions. Also in Figure 1, the cumulative charge around Ti^{n+} within a sphere of a given radius is shown; this charge converges to 4, 3, 2, and 1 e for Ti^0 , Ti^+ , Ti^{2+} , and Ti^{3+} , respectively.

Two qualitative features of the spherically averaged radial valence density can be identified with all methods: first, a local maximum of electron density at a radial distance of approximately 0.2–0.4 Å from the nucleus, which corresponds to d-type contributions because it is present even in the absence

of s-type valence density; second, a local maximum of the averaged valence density close to the Ti nuclear position, whose occurrence is connected to remaining s-contributions because the radial node of basis functions with $l > 0$ leads to a steep decrease and vanishing of d-type density close to the nucleus. The cumulative charges show that a significant fraction of the overall charge is contained in a sphere including the s- and d-type peaks, and it integrates to unity between 0 and 0.6 or 0.9 Å for Ti^0 or Ti^{2+} , respectively. The lack of valence electrons in Ti^{4+} results in a zero average valence density over the whole space. In the case of an eventually occurring, fully oxidized Ti center in TiO_2 compounds, no peak at $r \rightarrow 0$ nor a peak between 0.2 and 0.4 Å is expected.

For a TiO_2 molecule, the lowest-energy geometry obtained with B3LYP/cc-pVDZ (see Computational Details in the Supporting Information) is a bent structure with a Ti–O distance of 1.635 Å and a bond angle of 111.75°. Because O–Ti–O angles in rutile are either 90 or 180° and in anatase they are around 77, 102, and 180°, we decided to include a linear

molecular species as another model system as well. Although not a local minimum of the potential energy surface (PES), a linear structure with a Ti–O distance of 1.699 Å, lying about 2 eV above the bent species, was identified as a saddle point on the molecular PES. The obtained parameters are in good agreement with previously reported molecular geometries of TiO₂.²⁶ Figure 2 shows the spherically averaged radial valence density for both geometries and the same methods utilized for the isolated ions (see Computational Details in the Supporting Information).

As can be seen in Figure 2, a local maximum of the density in the vicinity of the Ti nucleus as well as a local maximum at around 0.3 Å from Ti occurs in both cases and for all used methods. This is similar to the case of Ti ions shown in Figure 1. Also similarly to the case of Ti ions, the cumulative charge reaches unity at around 0.7 Å, including most of the identified Ti s- and d-type density contributions, suggesting one remaining Ti electron at the metal center within a sphere with a radius of approximately 40–43% of the Ti–O bond length.

The resulting curve in Figure 2 for CAS-SCF is scaled by a factor of 0.3 for better comparison. The CAS(16,14) values show noticeable deviations from the other methods, predicting an even larger density remainder at the Ti atom, indicating again a strong influence of static correlation, which is expected to be lower in the octahedrally coordinated Ti in periodic systems. Despite obvious quantitative deviations, the CAS-SCF curve shows the above-mentioned characteristic points; the pronounced cusp-like maximum at $r = 0$ is not very visible due to the grid resolution. Remaining electron density on Ti is also predicted by the three types of charge analyses chosen, as shown in Table 1.

Table 1. Mulliken, Bader, and Hirshfeld Charges on Titanium for the Linear and Bent Configurations of the TiO₂ Molecule Obtained with B3LYP, CAS(16,14), CCSD, and PBE with the cc-pVDZ Basis Set

system/method		Mulliken	Bader	Hirshfeld
linear	B3LYP	+0.80	+2.45	+0.99
	CAS(16,14)	+0.86	+2.02	+1.12
	CCSD	+0.79	+2.61	+1.02
	PBE	+0.73	+2.34	+0.93
bent	B3LYP	+0.66	+2.15	+0.86
	CAS(16,14)	+0.74	+1.88	+0.89
	CCSD	+0.67	+2.25	+0.90
	PBE	+0.59	+2.05	+0.80

The charge measures vary significantly among different charge analysis methods, while they agree well between different electronic structure methods used for the same charge analysis method. For oxygen, the respective values obtained were approximately –0.3 with Mulliken, –1.1 with Bader, and –0.5 with Hirshfeld charge analysis (for a list of all oxygen values, see Table S1 in the Supporting Information).

To exclude the possibility of the shown valence density increase at the Ti center being predominantly caused by diffuse O-centered functions, the spherically averaged valence density of an oxygen dimer in the same relative alignment as in the linear species was computed for different reduced states (O₂, O₂[–], O₂^{2–}, O₂^{3–}, O₂^{4–}), with $r = 0$ being at the center of the elongated O₂ molecule or molecule ion (where the Ti atom would have been in a linear TiO₂ molecule). In this representation, it can be seen that the spherically averaged valence density of the O dimer is decreasing toward the center of the bond and not showing any peaks at around $r = 0$ for any oxidation state (see Figure S1 in the Supporting Information). This leads to the conclusion that the increase in valence density at the Ti center in TiO₂ is indeed caused by remaining charge density on titanium.

The Mulliken and Hirshfeld charges indicate significant contributions of Ti-centered basis functions to the electron density, as already expected from the averaged radial valence density plots, and differ significantly from the expected +4 charge state. The Bader charge analysis predicts the lowest value for the remaining charge on the Ti center of all methods. The minimum distance of the dividing surface to the titanium atom is 0.69 Å for CCSD and 0.72 Å for B3LYP and PBE in the case of a linear molecule and 0.60 Å for CCSD as well as 0.59 Å for B3LYP and PBE in the bent molecule. Comparing these distances to the average density plots in Figure 2 makes clear that the Bader analysis includes the parts of the density previously identified as characteristic of the Ti center. The Bader maxima assigned to the Ti atoms are also in agreement with the radial maxima belonging to Ti shown in Figure 2, suggesting a correct partitioning of the electron density within the grid-based Bader charge analysis formalism (see Computational Details in the Supporting Information). Because CCSD, B3LYP, and PBE results do not differ significantly regarding density plots and charge analyses, PBE is assumed to be accurate for the purpose of charge analysis and is used in calculations on periodic systems discussed in the next section.

The Bader charge remainder at Ti in the linear TiO₂ molecule obtained with PBE and larger (aug-)cc-pVXZ (X = D,T,Q,S) basis sets were extrapolated to the basis set limit (see

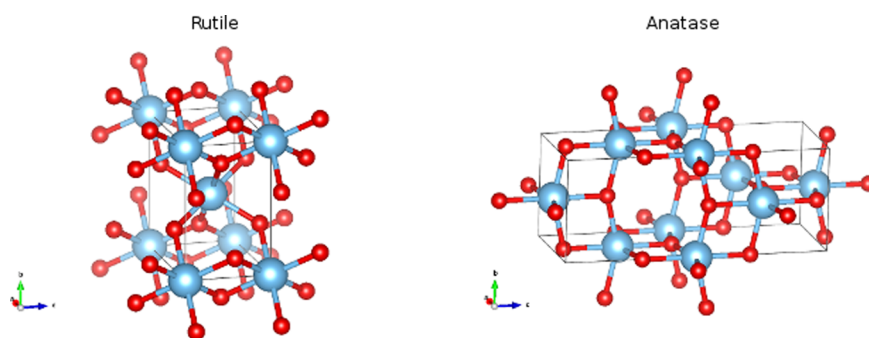


Figure 3. Optimized crystal structures of rutile (left) and anatase (right). Depicted are the unit cells used throughout this work; the blue spheres indicate Ti and red spheres represent O atoms.

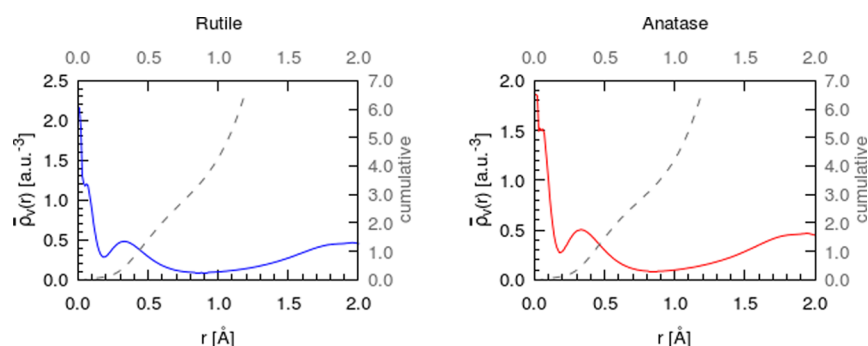


Figure 4. Spherically averaged valence electron density around the Ti atom of a periodic rutile and anatase structure calculated with PBE. The spatial coordinate r corresponds to the radial distance from one Ti center. The O atoms are located at $r = 1.96$ Å in rutile and $r = 1.95$ and 2.01 Å in anatase. The gray, dashed lines indicate the cumulative numbers of electrons within the spheres of corresponding radius.

Figure S2 and Computational Details in the [Supporting Information](#)). For both basis set series, the remaining charges at Ti converge to the same limit of +2.45, which corresponds to a deviation from the PBE/cc-pVDZ value of 4.3%. Although there is a small basis set influence, it can be stated that charges retrieved from the smaller basis set are in good agreement with the expected basis set limit.

The electronic structures of periodic anatase and rutile TiO_2 were obtained using full-potential all-electron calculations (see Computational Details in the [Supporting Information](#)). The relaxed geometries are in good agreement with available experimental and theoretical values: $a = 3.81$ Å (experimental:²⁷ 3.79 Å; theoretical (GGA):²⁸ 3.81 Å) and $c = 9.72$ Å (9.51 Å, 9.69 Å) for anatase and $a = 4.65$ Å (4.59 Å, 4.65 Å) and $c = 2.97$ Å (2.96 Å, 2.97 Å) for rutile. The structures were visualized using the software VESTA²⁹ and are shown in [Figure 3](#).

The Ti–O distances in the crystals are 1.96 Å in rutile; they are 1.95 and 2.01 Å in anatase. The spherically averaged valence densities around Ti for both systems are shown in [Figure 4](#). Once again, the plot exhibits a clear peak of $\rho_v(r)$ at the Ti position and a local maximum in its proximity (specifically, in the area of $r = 0.2$ – 0.5 Å identified above as coming from 3d Ti valence electrons), suggesting significant valence electron density remaining at the metal atom.

The cumulative charge integrates to unity at around 0.44 Å, including s- and d-type contributions, as in the molecule, but closer to the nucleus due to the increased charge density around the metal center caused by a larger number of coordinating oxygen ligands. Qualitatively, the picture does not change, and the data suggest one remaining electron within a small sphere confined to the metal center and a radius of now approximately 22% of the Ti–O distance. *This one-electron charge cannot be assigned to any other atom.* Similarly to the molecular case, Mulliken, Hirshfeld, and Bader population analyses were used on the periodic systems, and the results are summarized in [Table 2](#).

Table 2. Mulliken, Bader, and Hirshfeld Charge Analyses for a Ti Atom in the Periodic TiO_2 Structures Rutile and Anatase Calculated with PBE

system	Mulliken	Bader	Hirshfeld
rutile	+0.65	+2.52	+0.57
anatase	+0.65	+2.50	+0.55

The results differ only slightly from the molecular case with the values of Mulliken charges of Ti atoms in the crystals being between those of linear and bent configurations of the TiO_2 molecules, Hirshfeld charges being lower, and Bader charges being larger than those for the molecules. The corresponding charges for the oxygen atoms are approximately -0.3 with Mulliken and Hirshfeld as well as -1.3 with Bader charge analysis (for a list of all oxygen charges, see [Table S2](#) in the [Supporting Information](#)). However, once again, the data suggest a substantial remaining charge on the Ti atom that does not align with the conventional perception of the Ti^{4+} state in titanium dioxide compounds. This is in agreement with the observation that the TiO_2 valence band has noticeable Ti d-contributions, as can be seen in the l -projected partial density of states for Ti and O in rutile and anatase, as shown in [Figure S3](#) in the [Supporting Information](#). This observation is in agreement with PDOS plots of titania published in extensive theoretical literature.^{6,8,9} Also, similar results to those presented here regarding the DOS and charge analyses can be obtained by means of plane wave basis sets and using pseudopotentials.^{30,16}

As one can see, commonly used charge analysis schemes suggest that the titanium charge state in molecular and solid TiO_2 is between +0.6 and +2.6. The Bader charge analysis can be considered as the most reliable one in this sequence because it directly evaluates the electron density remainder around the nucleus and is therefore also directly related to the actual charge density; furthermore, the positions of zero-flux surfaces are in good agreement with the distance at which the cumulative charges integrate to unity. It is common to assign integer oxidation states to fractional computed charges. In many instances, there is a clear justification of such an assignment, based, for example, on the analysis of the band structure.^{22,31} In the case of TiO_2 , however, there is no solid justification for assigning, for example, the Bader charge of about $+2.5 e$ to a state Ti^{4+} . Yet, such a charge state is implied in the oxidation state that has been universally assumed in the literature as it implies that no further oxidation of the Ti atom is possible. Here, we performed comprehensive analysis of the electronic structure of Ti ions, TiO_2 molecules, and TiO_2 solids; valence density distribution, cumulative charge, and the employed charge analysis schemes suggest, in combination with the l -projected PDOS, a charge state of +3 for Ti. The respective charge state of oxygen would therefore correspond to -1.5 . While there is certain latitude in defining what an oxidation state is, we see no reasonable argument by which to assign an oxidation state of +4 to an atom with four valence electrons of which one remains at the atom and far from the

bonding region. We think that there is need to reconsider the assumed Ti oxidation state in TiO₂, at least in the framework of computational treatment. This is of particular interest in the case of redox processes in TiO₂ systems; for example, the assignment of oxidation states obtained in doped TiO₂ is done off of the assumed Ti⁴⁺ state in pure TiO₂.^{32–34} Our results suggest that, in principle, further oxidation at the Ti centers may be possible. Conversely, it follows that oxygen could be further reduced; indeed, oxygen redox activity is a known effect occurring, for example, upon Li intercalation in several cathode materials.³⁵

■ ASSOCIATED CONTENT

Supporting Information

The Supporting Information is available free of charge on the ACS Publications website at DOI: 10.1021/acs.jpcllett.7b00313.

Computational methods, oxygen charges in TiO₂ molecules and crystals, spherically averaged density of oxygen dimers, basis set extrapolated Bader charges, and *l*-projected partial DOS of rutile and anatase (PDF)

■ AUTHOR INFORMATION

Corresponding Author

*E-mail: mpemanzh@nus.edu.sg. Tel: +65 6516 4605. Fax: +65 6779 1459.

ORCID

Sergei Manzhos: 0000-0001-8172-7903

Notes

The authors declare no competing financial interest.

■ ACKNOWLEDGMENTS

This work was supported by the Ministry of Education of Singapore (Grant No. MOE2015-T2-1-011).

■ REFERENCES

- (1) Nakata, K.; Fujishima, A. TiO₂ Photocatalysis: Design and Applications. *J. Photochem. Photobiol., C* **2012**, *13*, 169–189.
- (2) Frank, A. J.; Kopidakis, N.; van de Lagemaat, J. Electrons in Nanostructured TiO₂ Solar Cells: Transport, Recombination and Photovoltaic Properties. *Coord. Chem. Rev.* **2004**, *248*, 1165–1179.
- (3) Schneider, J.; Matsuoka, M.; Takeuchi, M.; Zhang, J.; Horiuchi, Y.; Anpo, M.; Bahnemann, D. W. Understanding TiO₂ Photocatalysis: Mechanisms and Materials. *Chem. Rev.* **2014**, *114*, 9919–9986.
- (4) Liu, J.; Wang, J.; Ku, Z.; Wang, H.; Chen, S.; Zhang, L.; Lin, J.; Shen, Z. X. Aqueous Rechargeable Alkaline Co_xNi_{2–x}S₂/TiO₂ Battery. *ACS Nano* **2016**, *10*, 1007–1016.
- (5) Oh, S.-M.; Hwang, J.-Y.; Yoon, C. S.; Lu, J.; Amine, K.; Belharouak, I.; Sun, Y.-K. High Electrochemical Performances of Microsphere C-TiO₂ Anode for Sodium-Ion Battery. *ACS Appl. Mater. Interfaces* **2014**, *6*, 11295–11301.
- (6) Mo, S.-D.; Ching, W. Y. Electronic and Optical Properties of Three Phases of Titanium Dioxide: Rutile, Anatase, and Brookite. *Phys. Rev. B: Condens. Matter Mater. Phys.* **1995**, *51*, 13023–13032.
- (7) Glassford, K. M.; Chelikowsky, J. R. Structural and Electronic Properties of Titanium Dioxide. *Phys. Rev. B: Condens. Matter Mater. Phys.* **1992**, *46*, 1284–1298.
- (8) Scanlon, D. O.; Dunnill, C. W.; Buckeridge, J.; Shevlin, S. A.; Logsdail, A. J.; Woodley, S. M.; Catlow, C. R. A.; Powell, M. J.; Palgrave, R. G.; Parkin, I. P.; et al. Band Alignment of Rutile and Anatase TiO₂. *Nat. Mater.* **2013**, *12*, 798–801.
- (9) Rubio-Ponce, A.; Conde-Gallardo, A.; Olguín, D. First-Principles Study of Anatase and Rutile TiO₂ Doped with Eu Ions: A Comparison of GGA and LDA+U Calculations. *Phys. Rev. B: Condens. Matter Mater. Phys.* **2008**, *78*, 35107.

(10) Rogers, D. B.; Shannon, R. D.; Sleight, A. W.; Gillson, J. L. Crystal Chemistry of Metal Dioxides with Rutile-Related Structures. *Inorg. Chem.* **1969**, *8*, 841–849.

(11) Tossell, J. A.; Vaughan, D. J. Electronic Structure of Rutile, Wustite, and Hematite from Molecular Orbital Calculations. *Am. Mineral.* **1974**, *59*, 319–334.

(12) Scrocco, M. X-Ray Photoelectron Spectra of Ti⁴⁺ in TiO₂. Evidence of Band Structure. *Chem. Phys. Lett.* **1979**, *61*, 453–456.

(13) Fleming, L.; et al. Local Bonding Analysis of the Valence and Conduction Band Features of TiO₂. *J. Appl. Phys.* **2007**, *102*, 033707.

(14) Mulliken, R. S. Electronic Population Analysis on LCAO–MO Molecular Wave Functions. I. *J. Chem. Phys.* **1955**, *23*, 1833–1840.

(15) Bader, R. F. W. Atoms in Molecules. *Encyclopedia of Computational Chemistry*; John Wiley & Sons, Ltd.: Chichester, U.K., 2002.

(16) Arrouvel, C.; Parker, S. C.; Islam, M. S. Lithium Insertion and Transport in the TiO₂–B Anode Material: A Computational Study. *Chem. Mater.* **2009**, *21*, 4778–4783.

(17) Daude, N.; Gout, C.; Jouanin, C. Electronic Band Structure of Titanium Dioxide. *Phys. Rev. B* **1977**, *15*, 3229–3235.

(18) Chauque, S.; Robledo, C. B.; Leiva, E. P. M.; Oliva, F. Y.; Cámara, O. R. Comparative Study of Different Alkali (Na, Li) Titanate Substrates as Active Materials for Anodes of Lithium - Ion Batteries. *ECS Trans.* **2014**, *63*, 113–128.

(19) Wu, L.; Bresser, D.; Buchholz, D.; Giffin, G. A.; Castro, C. R.; Ochel, A.; Passerini, S. Unfolding the Mechanism of Sodium Insertion in Anatase TiO₂ Nanoparticles. *Adv. Energy Mater.* **2015**, *5*, 1401142.

(20) Karen, P.; McArdle, P.; Takats, J. Comprehensive Definition of Oxidation State (IUPAC Recommendations 2016). *Pure Appl. Chem.* **2016**, *88*, 831–839.

(21) Legrain, F.; Manzhos, S. Aluminum Doping Improves the Energetics of Lithium, Sodium, and Magnesium Storage in Silicon: A First-Principles Study. *J. Power Sources* **2015**, *274*, 65–70.

(22) Liu, W.; Sk, M. A.; Manzhos, S. Grown-in Beryllium Diffusion in Indium Gallium Arsenide: An Ab Initio, Continuum Theory and Kinetic Monte Carlo Study. *Acta Mater.* **2017**, *125*, 455.

(23) Hirshfeld, F. L. Bonded-Atom Fragments for Describing Molecular Charge Densities. *Theor. Chim. Acta* **1977**, *44*, 129–138.

(24) Saloman, E. B. Energy Levels and Observed Spectral Lines of Neutral and Singly Ionized Titanium, Ti I and Ti II. *J. Phys. Chem. Ref. Data* **2012**, *41*, 013101.

(25) Sugar, J.; Corliss, C. *Atomic Energy Levels of the Iron-Period Elements: Potassium through Nickel*; American Chemical Society: New York, United States, 1985.

(26) Lin, C.-K.; Li, J.; Tu, Z.; Li, X.; Hayashi, M.; Lin, S. H. A Theoretical Search for Stable Bent and Linear Structures of Low-Lying Electronic States of the Titanium Dioxide (TiO₂) Molecule. *RSC Adv.* **2011**, *1*, 1228–1236.

(27) Cromer, D. T.; Herrington, K. The Structures of Anatase and Rutile. *J. Am. Chem. Soc.* **1955**, *77*, 4708–4709.

(28) Arroyo-de Dompablo, M. E.; Morales-García, A.; Taravillo, M. DFT+U Calculations of Crystal Lattice, Electronic Structure, and Phase Stability under Pressure of TiO₂ Polymorphs. *J. Chem. Phys.* **2011**, *135*, 054503.

(29) Momma, K.; Izumi, F. VESTA 3 for Three-Dimensional Visualization of Crystal, Volumetric and Morphology Data. *J. Appl. Crystallogr.* **2011**, *44*, 1272–1276.

(30) Zhang, J.; Zhou, P.; Liu, J.; Yu, J. New Understanding of the Difference of Photocatalytic Activity among Anatase, Rutile and Brookite TiO₂. *Phys. Chem. Chem. Phys.* **2014**, *16*, 20382–20386.

(31) Legrain, F.; Manzhos, S. A First-Principles Comparative Study of Lithium, Sodium, and Magnesium Storage in Pure and Gallium-Doped Germanium: Competition between Interstitial and Substitutional Sites. *J. Chem. Phys.* **2017**, *146*, 034706.

(32) Di Valentin, C.; Finazzi, E.; Pacchioni, G.; Selloni, A.; Livraghi, S.; Paganini, M. C.; Giamello, E. N-Doped TiO₂: Theory and Experiment. *Chem. Phys.* **2007**, *339*, 44–56.

(33) Colón, G.; Maicu, M.; Hidalgo, M. C.; Navío, J. A. Cu-Doped TiO₂ Systems with Improved Photocatalytic Activity. *Appl. Catal., B* **2006**, *67*, 41–51.

(34) Morita, K.; Shibuya, T.; Yasuoka, K. Stability of Excess Electrons Introduced by Ti Interstitial in Rutile TiO₂(110) Surface. *J. Phys. Chem. C* **2017**, *121*, 1602–1607.

(35) Seo, D.-H.; Lee, J.; Urban, A.; Malik, R.; Kang, S.; Ceder, G. The Structural and Chemical Origin of the Oxygen Redox Activity in Layered and Cation-Disordered Li-Excess Cathode Materials. *Nat. Chem.* **2016**, *8*, 692–697.